An X-ray absorption study of gold coordination compounds: EXAFS refinements and double electron excitation background

1994 J. Phys.: Condens. Matter 6 8429

(http://iopscience.iop.org/0953-8984/6/41/007)

J. Phys.: Condens. Matter 6 (1994) 8429–8448. Printed in the UK

An x-ray absorption study of gold coordination compounds: EXAFS refinements and double-electron excitation background

R E Benfield†, A Filipponi†‖, D T Bowron‡, R J Newport‡ and S J Gurman§

† Chemical Laboratory, University of Kent at Canterbury, Canterbury CT2 7NH, UK
‡ Physics Laboratory, University of Kent at Canterbury, Canterbury CT2 7NR, UK
§ Department of Physics and Astronomy, University of Leicester, Leicester LE1 7LH, UK

Received 13 June 1994, in final form 15 August 1994

Abstract. X-ray absorption spectra at the Au L edges of $Au(PPh_3)Cl$, $Au(PPh_3)_2Cl$ and $KAuCl_4 \cdot 2H_2O$ have been collected as a function of temperature. Data analysis of the extended x-ray absorption fine structure was carried out with the GNXAS package performing an appropriate treatment of the multiple-scattering effects involving several ligand atoms. The accuracy of the current analysis procedures for the Au L edges is assessed and the sensitivity to coordination numbers and distances is established. Evidence for the presence of a [2p4f] double-electron excitation in the atomic Au background is obtained for the first time. The results presented in this paper are of general importance for improving data analysis at the Au L edges and in particular for improving the EXAFS results in Au cluster compounds.

1. Introduction

Gold, although regarded as the archetypal 'noble metal', has a quite extensive chemistry [1, 2]. There are many coordination compounds of Au^I, which mostly have linear two-coordinate geometries, and of Au^{III}, which commonly have the four-coordinate square planar geometry characteristic of d^8 metal ions. Several of these compounds are under active investigation as anti-arthritic drugs. In order to probe the local structure or the relevant interaction site for the Au atoms, extended x-ray absorption spectroscopy (EXAFS) has often been used [3].

Gold also forms a wide range of cluster compounds, containing typically 11 or 13 gold atoms [4]. These are of special interest because many of their cluster structures, characterized by x-ray crystallography, are based on icosahedral geometries, which are not possible in bulk metal lattices. Gold colloids, synthesized by chemical reduction of Au^{III} salts in solution, have also been the subject of study for many years [5]. New methods of size control of these colloidal particles down to 20 Å diameter and below are still being sought [6].

Intermediate between the crystallographically characterized cluster compounds of gold and the gold colloids is a range of high-nuclearity gold cluster compounds. The most extensively studied example is $Au_{55}(PPh_3)_{12}Cl_6$ [7], where PPh_3 denotes the

‖ Permanent address: Dipartimento di Fisica, Università degli Studi dell'Aquila, Via Vetoio, 67010 Coppito, L'Aquila, Italy.

0953-8984/94/418429+20$19.50

triphenylphosphine ligand. A wide range of spectroscopic methods has been applied to this material, and its physical properties have been closely studied [8]. The bonding in $Au_{55}(PPh_3)_{12}Cl_6$ has been shown to be much more delocalized, non-directional and metallic in character than in smaller gold cluster compounds [9].

$Au_{55}(PPh_3)_{12}Cl_6$ and related clusters pack amorphously in the solid state, and it has not proved possible to grow crystals suitable for x-ray crystallography. Their structures have been extensively studied by Au L_3 edge EXAFS spectroscopy [10, 11, 12, 13]. These EXAFS analyses have shown that $Au_{55}(PPh_3)_{12}Cl_6$ has a cuboctahedral cluster structure, and that the Au–Au distances in the cluster are substantially shorter than those in bulk gold. Metal–ligand (Au–P and Au–Cl) distances have also been resolved. The shape of the x-ray absorption edge shows qualitatively that the gold atoms in $Au_{55}(PPh_3)_{12}Cl_6$ have a mean oxidation state close to that in the bulk metal.

However, there are several unresolved aspects of these EXAFS studies. The assignment of Au–P and Au–Cl distances was hindered by the lack of EXAFS data on suitable crystallographically characterized reference compounds of gold containing phosphine and chloride ligands. Additionally, a more quantitative evaluation of the mean oxidation state of the gold atoms in $Au_{55}(PPh_3)_{12}Cl_6$ requires analysis of the 'white lines' in the Au L_3 and L_2 edge XAS spectra of the cluster and a series of reference materials of known oxidation state [14].

The commonly used EXAFS data analyses at the Au L_3 edge have been always based on rather simple EXAFS theories and methodologies, including the single-scattering approximation and the use of empirical fits. The limitations of these methods were recognized early [15] in comparison with the results of crystallographic data. It is our opinion that the use of more advanced EXAFS data analysis, based on theoretical standards rather than on experimental ones, is nowadays feasible, and that once these methods have been established and their accuracy has been put to the test, which is the main purpose of the present investigation, all of the several applications of this Au edge spectroscopy will be strongly advantaged.

Another quite interesting subject of research with both fundamental and applied aspects is the identification and understanding of multi electron excitation effects hidden in the atomic absorption background. While these effects have been known and investigated for many years by atomic physicists in noble gases or monatomic vapour phase samples (see [16] and references therein), the existence of similar effects in the cross-section of embedded atoms in condensed matter, and the relevance of the understanding of these phenomena for the improvement of the EXAFS data analysis has been pointed out only in relatively recent times ([17, 18, 19] and references therein). The suggestion that double-electron excitation effects can be intense at the Au L edges comes from the previous investigations performed on other sixth-period elements. In a careful study of Hg vapours [20] a slope change around 135 eV above the L_3 and L_2 edges was clearly observed, and identified as the effect of the onset of the [2p4f] double-electron excitation channels. In a successive study dealing with pure elements and compounds of Pb, Bi [21] the same effects have been detected at progressively higher energies with respect to the L edges, in agreement with theoretical predictions based on differences of self-consistent calculations ΔSCF. The interplay between these double-electron excitation features and the EXAFS signal was previously investigated at the Pb L_3 edge of PbO_2 [22]. Previous EXAFS investigations at the Au L_3 edge [15, 23] indicated the difficulty in accounting properly for the atomic background and removing all of the spurious low-distance peaks in the Fourier transform. Following these previous findings it is expected that double-electron excitation effects are indeed present also at the Au L edges, although their identification is certainly hampered by the smaller energy difference

with respect to the main edge and by the intensity of the EXAFS oscillations present in solid Au compounds.

In the present investigation we have studied Au L edge XAS spectra of three coordination compounds of gold with structures known from x-ray crystallography. These are $Au(PPh_3)Cl$, a linear compound of Au^I [24]; $Au(PPh_3)_2Cl$, a trigonally coordinated compound of Au^I [25, 26]; and $KAuCl_4 \cdot 2H_2O$, a square planar complex of Au^{III} [27]. The first two, to the best of our knowledge, have never been studied by EXAFS, while the latter has been previously measured [28], in the context of a study of Au in aqueous solutions, and has often been quoted as the reference compound used to isolate the Au–Cl contribution. The structural information derived from refinement of the EXAFS data from these compounds is critically compared with their crystallographic parameters. The results of this analysis provide a full insight into the potential of the current EXAFS data analysis method applied to Au compounds, and will underpin the EXAFS analysis of Au clusters.

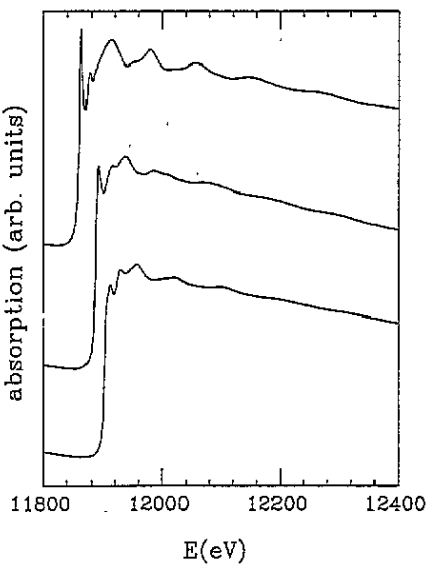

Figure 1. Au L_3 x-ray absorption spectra of $Au(PPh_3)Cl$, 295 K (bottom), $Au(PPh_3)_2Cl$, 80 K (middle) and $KAuCl_4 \cdot 2H_2O$ 80 K (top). The energy scale for the latter two spectra has been displaced for clarity.

2. Experimental details

$Au(PPh_3)Cl$ (99.9+%) was purchased from Aldrich. Unsolvated $Au(PPh_3)_2Cl$ was synthesized by reaction of $Au(PPh_3)Cl$ with PPh_3 in ethanol [29]. The product had satisfactory microanalysis and melting point. $KAuCl_4 \cdot 2H_2O$ (assay 51.45% Au) was purchased from Johnson–Matthey.

Measurements were carried out using the 7.1 beamline (SRS—Daresbury Laboratory). The beamline was equipped with a Si (111) double-crystal monochromator with a feedback system to maintain higher-order harmonic rejection. The crystals were detuned setting the intensity to 50% of the peak maximum. The ring was operating at 2.0 GeV with typical currents in the 200 mA range. Temperatures were controlled with a liquid nitrogen cryostat (Oxford Instruments). For all three compounds spectra were collected at 80 K, and for

$Au(PPh_3)Cl$ data were also obtained at 190 K and 295 K.

Typical L_3 edge spectra for the three compounds under consideration are reported in figure 1.

3. Data analysis

EXAFS data analysis has been performed by using the GNXAS method [30, 31] that presents several important features that can be particularly useful to study EXAFS spectra of these Au compounds.

The main characteristics of the GNXAS package is the possibility of accounting for the multiple-scattering (MS) effects associated with triplet configurations to any order in the scattering. This is accomplished by means of a continued fraction expansion algorithm [32] that presents improved convergence properties with respect to the usual MS series [33].

The vibrational damping of MS signals is performed by using correlated vibration matrices describing the mean square displacements of groups of atoms involved. In addition GNXAS has shown a high flexibility in modelling atomic backgrounds due to the possibility of accounting for double-electron excitation channels [17, 18].

3.1. Phase shifts and signals

Theoretical details on the prescription and approximation used to model a complex effective potential for the photoelectron used within the GNXAS scheme have been reported elsewhere [34]. Accurate phase shifts (up to $E_{Max} = 100$ Ryd above the edge, including $\ell_{Max} = 25$) have been calculated for all the atoms involved in the three model compounds. The potential calculation, within a muffin tin scheme, is based on spherically averaged overlapped atomic potentials. The overlapped charge densities take account of the shells of the closest ligands reproducing the correct chemical environment of each scatterer. In the present case this information is clearly known from the crystal structures; these atomic phase shifts, however, are largely transferable to systems with similar ligands and charge transfers.

The muffin tin radii have been chosen in agreement with standard prescriptions [34], and are approximately given by 75% of the Norman radii; care has been taken to avoid large overlaps. The used radii were 1.23 Å for Au, 1.00 Å for P, 1.11 Å for Cl and 0.74 Å for C. C is present largely in phenyl rings and the 0.74 Å radius guarantees a small overlap. These radii were found to generate a consistent set of potentials for the analysis of all the reference Au compounds.

Structural signals associated with the various coordination shells were calculated using the GNXAS code. Among these, particularly relevant to the present study were the Au–P and Au–Cl contributions, the latter presenting a wider distance spread among different compounds.

Multiple-scattering effects were found to be detectable in various cases, as specified below. In particular aligned configurations of different ligands are clearly seen by the EXAFS spectroscopy. These occur for instance in the $AuCl_4$ planar configuration as well as in the P–Au–Cl linear configuration. Other triplet contributions were calculated for the Au–P–C triangles, C being the C atom from bonded phenyl rings. The signals associated with all these three-body configurations including MS to any order in the scattering have been calculated with the continued fraction expansion algorithm [32].

3.2. Fitting procedure

In order to assess the magnitude of the systematic errors associated with the data analysis method, that is based on theoretical standards, we performed fits of model signals, associated with appropriate model structures, to the experimental EXAFS spectra. The results of the refinement of the structural parameters were successively compared with the known crystallographic results showing the errors of the data analysis in these known systems, but providing also an insight into the sensitivity of the technique in the case of unknown compounds. The analysis was performed with the FITHEO program (GNXAS package) using the previously calculated contributions from separate units. Statistical errors in the fitting parameters have been evaluated using 95% confidence intervals in the multi-dimensional parameter space, accounting for possible correlations as described elsewhere [31].

In typical EXAFS data analysis methods there are several empirical parameters that affect the signal shape (especially the amplitude) that can be varied to some extent. It is quite important to fix them to reasonable values in order to get reliable structural results. In our scheme the photoelectron damping and core hole lifetime effects have been included in the model potential as described in the previous section. The experimental resolution function is another damping parameter that might affect the intensity of the signal at low k, that should be accounted for. We worked out an independent experimental determination of the energy resolution based on fit of the L edge rise in several Au compounds. Due to the steepness of the edge features we could easily determine the standard deviation of a Gaussian function that convoluted with model spectra was able to represent appropriately the experimental resolution function. The optimal standard deviation value was found to be 0.6(2) eV, the uncertainty arises mainly by the dominance of the core hole width that is 6 eV full width at half maximum.

The only empirical parameter that was actually released was the so called S_0^2 factor. This accounts for a uniform reduction of the signal amplitude possibly associated with many-body effects. In the present case where the coordination numbers are known the results can be actually used to calibrate the S_0^2 parameter for Au L edges to be transferred to the analysis of other unknown compounds. The latter values always refined in the range $S_0^2 = 0.85(5)$ for all edges and compounds being examined.

EXAFS Debye–Waller (DW) factors are known to provide a Gaussian damping in k space of the type $W(k) = \exp(-2\sigma^2 k^2)$ for a single-scattering contribution. We shall mainly refer to the variance of the bond distance distribution σ^2 in the following. In the harmonic approximation the total σ^2 is given by the sum of two contributions: $\sigma^2 = \sigma_T^2 + \sigma_{Str}^2$. The term σ_T^2 is the mean square vibrational amplitude associated with thermal motion and is temperature dependent, σ_{Str}^2 is a contribution associated with structural disorder among a set of equivalent bonds that are not separated in the analysis. The σ_{Str}^2 term can be calculated from the equilibrium positions of the atoms known from the crystal structure.

In the case of systems with many different shells with similar distances σ^2 parameters can be strongly correlated in the fit, it is therefore necessary to limit their variation range within reasonable limits. There are lower and upper limits to be accounted for. The thermal component has a lower limit associated with the zero-point vibrations. Well established methods exist to calculate the vibrational mean square amplitudes in molecules [35] as a function of temperature. In the cases when a force constant model is not available the whole $\sigma_T^2(T)$ function can be roughly estimated using an effective Einstein model for the bond vibration [36].

$$\sigma_T^2(T) = \frac{\hbar}{2\mu\omega} \coth\left(\frac{\beta\hbar\omega}{2}\right) \tag{1}$$

where $\beta = 1/k_B T$, ω is the effective Einstein frequency and μ is the reduced mass of the bond. The previous equation is exact for a one-dimensional harmonic osillator, but, to a good degree of approximation, it can be extended to bond stretching vibration in complex molecules. In this case an estimate for the effective Einstein frequency can be provided by IR studies of the system where clear vibrational modes have been assigned to the bond stretching under consideration.

In the following subsections details for each of the model compounds are reported.

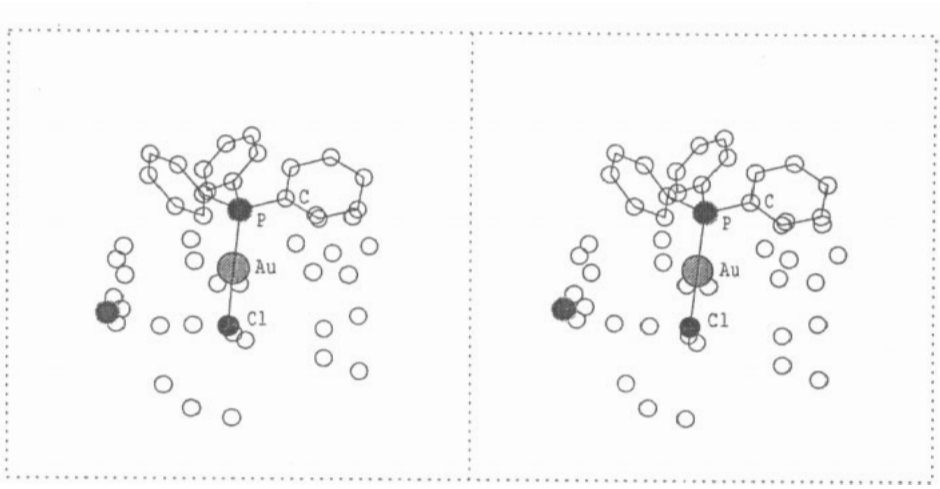

Figure 2. Stereoscopic direct view of the environment of the Au atom in $Au(PPh_3)Cl$ up to 5.0 Å; the molecular unit is evidenced by the chemical bonds reported as solid lines.

3.3. $Au(PPh_3)Cl$ and double-electron excitation

Among the existing gold compounds $Au(PPh_3)Cl$ is certainly one of the most attractive for calibrating EXAFS data analysis procedures and especially the absorption background at the Au L edges. The crystalline structure of $Au(PPh_3)Cl$ is known [24] and according to the space group $P2_12_12_1$ there are four equivalent molecules in the unit cell. A stereoscopic view of the environment of the Au atom up to 5.0 Å is shown in figure 2. Intermolecular contacts, as seen from the Au atom, are relatively long distance so that the EXAFS spectrum predicted by the theory is dominated by a few intramolecular contributions. The closest atom to Au is a P of the bonded triphenylphosphine at about 2.23 Å, followed by the Cl at about 2.28 Å and by three C atoms at 3.4 Å of the phenyl rings, directly bonded to the P. From this distance onwards there is a large number of intramolecular and intermolecular Au–C distances with practically a uniform distribution that is not likely to generate a visible EXAFS. The structural analysis however should be also extended to possible triplet configurations; for instance the Au–P–C contribution should be considered since it is expected to be comparable with the direct Au–C pair signal. In addition particular attention should be paid to the triplet P–Au–Cl linear configuration, that is expected to generate a rather intense MS signal. The bare signals calculated without taking account of the configurational average damping are shown in figure 3.

The signals have been used in the successive fitting procedure including possible distance refinements and consideration of the configurational average effects to reproduce the observed EXAFS spectrum. We performed a preliminary analysis of the room temperature

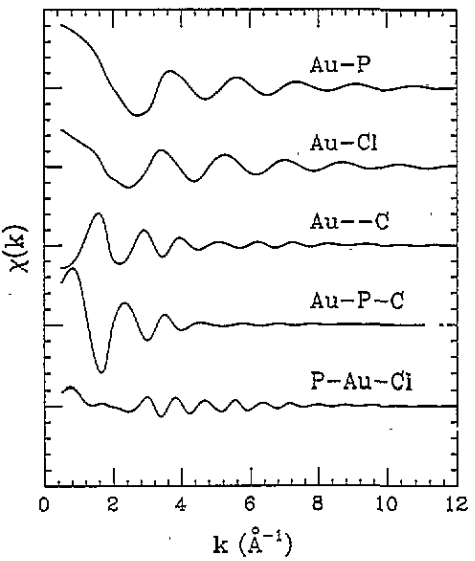

Figure 3. Theoretical $\chi(k)$ signals for the main two-body and three-body configurations in $Au(PPh_3)Cl$. They have been calculated for the crystallographic distances and no account has been taken of the configurational average. From top to bottom the figure reports Au–P, Au–Cl and Au–C two-body signals and Au–P–C and P–Au–Cl three-body multiple-scattering contributions. The signals are shifted for clarity by 0.1 units along the y axis. The degeneracy of the configurations has been taken into account, being three when the C atom is involved and unity elsewhere.

spectrum using a standard polynomial spline to model the atomic background beyond the Au edge. The results are shown in figure 4 for the $k\chi(k)$ data (upper panel) and magnitude of the Fourier transform (FT) (lower panel). While the agreement between experiment and calculated data might seem satisfactory a rapid analysis of the residual reveals a clear pattern with a cusp at $k = 5.4$ Å^{-1}, indicated by the arrow, corresponding to an energy of $\Delta E = 110 \pm 5$ eV above the L_3 threshold. The cusp is actually associated with a clear slope change that after a careful inspection is visible even in the raw absorption data (figure 1). The polynomial spline is not able to account for such a slope discontinuity and produces the residual pattern shown in figure 4. The effect in the Fourier transform is, as expected, the presence of a broad feature peaking at very low distances (arrow in lower panel) which cannot be associated with any physical structural effect. This phenomenology is nowadays quite familiar in EXAFS spectra, and is characteristic of the effects of the opening of a double-electron excitation channel in the presence of structural contributions. Similar effects were observed in Br_2 [17], brominated hydrocarbon molecules [18] and many other compounds. In addition previous studies at L edges of sixth-period elements have definitely proven the presence of a slope change in the background associated with the simultaneous excitation of a $2p_{3/2}$ and a 4f electron. These investigations dealt with vapour Hg [20], liquid Pb and Bi and some Pb and Bi compounds [21]. In all cases the intensity of the structural signal was rather negligible. The present analysis, summarized in figure 4, provides the first direct experimental evidence for the presence of the $[2p_{3/2}4f]$ excitations at the Au L_3 edge. The energy position and the cusp are in perfect agreement with the theoretical predictions in the ΔSCF scheme [20, 21].

The present findings suggest that the EXAFS data analysis at the Au L edges can be

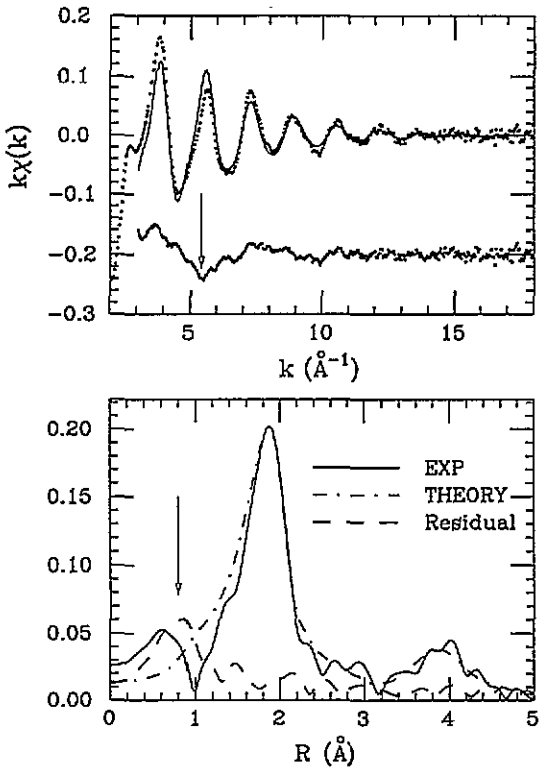

Figure 4. Evidence for the presence of the [$2p_{3/2}4f$] double-electron excitations in the Au L_3 edge background. Upper panel: $k\chi(k)$ signal for $Au(PPh_3)Cl$, experiment, 295 K, and model *(upper) and residual (lower). The residual clearly shows the presence of a cusp* (arrow) *at* $k = 5.4$ Å^{-1} corresponding to the double-excitation threshold. Lower panel: Magnitude of the Fourier transform of the $k\chi(k)$ signals, illustrating the unphysical low-R peak (arrow) in the residual FT.

improved if proper account is taken of such a double-electron background feature. Excluding for the moment the possibility of calculating the intensity of the double-electron channels, we have used an empirical approach to the problem. According to the prescriptions of the GNXAS method we generated a model background using appropriate empirical shapes according to a model function first introduced for the Br double-electron excitations [17].

When proper account is taken of the [$2p_{3/2}4f$] excitations the agreement of the calculated and experimental EXAFS signals is excellent as shown in figure 5. The empirical model background depends on only four other additional parameters, but the residual of the fit improved in a significant way, decreasing by even a factor of 0.5, confirming the statistical significance of these new parameters. Figure 5 shows in detail the various signals used to model the structural component of the spectrum. Notice that the signal labelled Au···C appears much weaker than the corresponding carbon signals in figure 3. This is because of the partial cancellation between pair and triplet signals and also because of the larger disorder terms. In practice the Au···C term accounts in an effective way for the large number of C atoms surrounding the Au atom starting from about 3.4 Å. The present analysis reveals, however, that under these conditions the EXAFS analysis is not able to locate any distinct group of C atoms around the Au. The magnitude of the Fourier transform (FT) for each of the four separate signals and for experiment, total model signal and residual, are presented

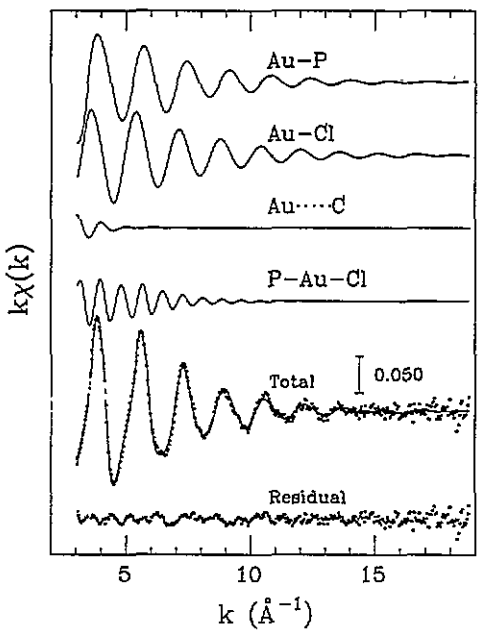

Figure 5. Best fit of the Au L_3 edge spectrum of $Au(PPh_3)Cl$ at 295 K. Each two-body and three-body contribution is reported as indicated by the labels. The large signal associated with the P–Au–Cl three-body configuration is peculiar to this linear structure. The comparison between total experiment and model signals is excellent, and the residual substantially contains experimental noise only.

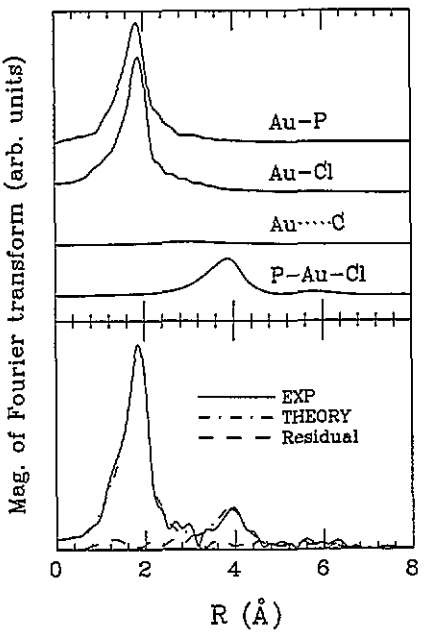

Figure 6. Magnitude of the Fourier transform of the signals reported in figure 5. The well defined high-frequency contribution from the P–Au–Cl configuration is essential to explain the experimental peak at 4 Å.

Table 1. Structural parameters for the $Au(PPh_3)Cl$ molecule obtained in the present EXAFS analysis and comparison with crystallographic results.

Configuration	Parameter	(units)	Crystal structure 300 K	L_3 P↔Cl 295 K	L_3 No IIexc 295 K	L_3 295 K	L_3 190 K	L_3 80 K	L_2 80 K	L_1 80 K
Au–P	R	(Å)	2.233	2.275(12)	2.27(2)	2.231(10)	2.232(8)	2.214(8)	2.24(2)	2.23(3)
	σ^2	(10^{-4} Å^2)		40(20)	36(20)	35(10)	25(10)	19(8)	<30	<40
Au–Cl	R	(Å)	2.278	2.256(25)	2.25(2)	2.281(10)	2.276(9)	2.277(6)	2.29(2)	2.27(3)
	σ^2	(10^{-4} Å^2)		80(30)	70(30)	33(10)	30(10)	12(6)	<20	<80
Au–C	R	(Å)	3.4	3.5(1)	3.4(2)	3.5(2)	3.7(2)	3.7(2)	3.7(2)	
P–Au–Cl	θ	(deg)	179.7	180(f)	180(f)	180(f)	180(f)	180(f)	180(f)	180(f)
	σ_θ^2	(deg^2)		<180	<150	<200	<160	90(80)	<130	
Residual		10^{-6}		5.9	9.4	5.6	4.4	5.1	4.8	20.5

in figure 6 (upper and lower curves respectively). A summary of the structural parameters obtained in the fitting procedure is reported in table 1, in comparison with diffraction results. The Au–P and Au–Cl pair signals clearly dominate the low-frequency part of the spectrum. Reliable values for the structural parameters can be obtained as compared with the known structure. The Au–C signal contributes mainly in a region around 2.8 Å in the FT, and the

fit improves slightly with its inclusion; however the C signal itself is not strong enough to allow an independent EXAFS determination of the C atom positions.

An interesting contribution, whose presence in the experimental FT in figure 6 is clearly visible, is the high-frequency peak at about 4.0 Å. In the real structure there is no atom or groups of atoms in this distance range able to generate such a signal and the only explanation for its origin is that it is a MS contribution. Our MS calculation for the P–Au–Cl configuration clearly demonstrates the importance of this contribution, and, in fact our calculated signal is able to account in a precise manner for both the amplitude and the phase of the high-frequency component. The theoretical fitted P–Au–Cl contribution is the fourth signal in figure 5.

We would like to emphasize again that the P–Au–Cl signal has been calculated with the continued fraction approach [32] that effectively includes MS terms to all orders in the scattering. This is evident in figure 6 where the fourth signal from the top corresponding to the P–Au–Cl signal actually has a main frequency contribution around 4 Å but it also contains a higher-frequency component around 6 Å associated with several χ_5 and χ_6 MS signals.

A brief comment should be made on the total number of parameters that are actually fitted to the spectra. According to previously published criteria [37] the number of parameters should be lower than limits established from the width of the spectrum in k and R spaces. The signal was fitted over a range of $\Delta k \approx 15$ Å^{-1}, while each of the low- and high-frequency peaks contribute to a region of about $\Delta R \approx 2$ Å. Therefore, for each peak we are allowed to fit about $(2/\pi)\,\Delta k\,\Delta R \approx 20$ parameters. Our total number of parameters is ten (14 including background) against 40. With only 14 parameters we are able to explain in a perfect way the experimental signal. The parameters are divided in the following way: four double-excitation background, four first-peak parameters (R and σ^2 for Au–P and Au–Cl), two for the C contribution, two MS peak additional vibration parameters (ρ, σ_θ^2), and two others (E_0 and S_0^2). The structural refinement of the damping of the signals provides an important information on the thermal disorder in the system. We point out that to account for the MS peak requires only two more parameters to be included since the rest are already fixed by the first-peak signals. The inclusion of the P–Au–Cl contribution reduces the residual by about the 20% that makes it statistically meaningful.

A similar analysis has been performed on L_3 spectra collected at 190 K and 80 K, as well as on the L_2 and L_1 edge spectra at 80 K. In the cases a perfect fit was obtained, the residual being always dominated by random noise. The results of all these measurements on $Au(PPh_3)Cl$ are summarized in table 1. The errors reported in parenthesis correspond to the 95% confidence interval of the combined ten structural parameters, (see [31] for details) and include the effect of their correlations. In some cases only upper or lower bounds could be obtained. A certain number of conclusions can be drawn.

(a) The EXAFS determinations of the Au–P and Au–Cl bond lengths are in perfect agreement with diffraction data, the sensitivity in the L_3 edge case is on the average slightly better than 0.01 Å.

(b) The main Au–P and Au–Cl contributions are clearly detected at both L_2 and even L_1 edges, although a lower accuracy is obtained in the distance determination than from the L_3 edge.

(c) The absolute σ^2 parameter can be measured and reasonable trends for the Au–P and Au–Cl values, compatible with an effective Einstein frequency for the vibration of both bonds in the 300 cm^{-1} range, are observed. By comparison, the stretching frequencies measured by IR spectroscopy are about 330 cm^{-1} for Au–Cl and 350 cm^{-1} for Au–P [38].

This very good agreement is strong evidence for the physical reliability of all the structural and thermal parameters obtained from our refinement.

(d) There is no sensitivity to Au···C distances and no useful numbers can be derived.

(e) The P–Au–Cl contribution is essential to improve the fitting and some information on the vibration of the unit can be obtained. As an example the P–Au–Cl angle has a relatively broad angular distribution with a root mean square deviation of about 10° around collinearity. EXAFS is able to detect mostly upper limits for the σ_θ^2 parameter that show, however, a clear temperature trend. The sensitivity to the correlation among the vibrations of the Au–P and Au–Cl bonds was found to be small, in this case, any number between -0.4 and +0.4 being acceptable; however on average there is a tendency towards slightly anticorrelated values ($\rho = -0.1$).

The inclusion of an appropriate background model with the double-electron excitation discontinuity is essential for accurate determination of the structural parameters. The results of the fitting of the 295 K data without double excitations, reported in table 1, indicate that large systematic errors occur. They amount in this case to even 0.04 Å in the short ligand distances, and in practice hamper the location of the correct minimum. This demonstrates once again the importance of including double-electron excitation effects in the background model. It should be pointed out, however, that this particular case is complicated by the weakness of the EXAFS and by the similarity of the P and Cl atoms as discussed below, and, therefore, such a failure of the conventional background model should not be taken as a general rule.

One of the purposes in the present investigation was to assess the EXAFS sensitivity to low-Z ligands of the Au atom. In the present sample there is a very difficult situation with two ligands, differing by only one unit in atomic number, at practically the same distance. The two corresponding oscillations are quite similar, although a shift in the total phase can be observed. There is no beating effect in the envelope, and it is expected that there is a large correlation between the structural parameters. Actually we found that with fixed coordination numbers, the minimum residual is associated with structural parameters which are in spectacular agreement with the crystallographic ones. It might be of interest to verify what is the actual sensitivity in the coordination numbers. We found that in floating these parameters they were always refined within 10% of the actual values. A final interesting problem is the actual sensitivity to the atomic types. In the space of the two distances Au–P and Au–Cl there must be two local minima associated with the exchange P↔Cl. Because of similarities in the bond distances these minima must be very close in parameter space. A very good fit could be in fact obtained with the constraint $R_{Au-P} > R_{Au-Cl}$, in practice exchanging the role of the two atoms, these results are also reported in table 1. We verified that the true minimum is actually deeper than the false one by about 5%; unfortunately this difference in the depth is not enough to be able to select the right minimum on solid statistical grounds. However, looking at the structural parameters, it is clear that in the wrong model the Au–Cl σ^2 value refines to a suspiciously too large value. Further insight in the minimum selection can be provided, in some cases, on the basis of external chemical knowledge, this will be discussed in the next example.

It should not surprise the reader that in over 20 years of extensive investigations at the Au L edges the presence of this feature has been so elusive. The difficulties of the background subtraction [15, 23] were, in any case, well recognized. However, in most cases the comparison was performed on Fourier filtered spectra where the typical pattern shown in figure 4 is lost, at the same time a high-k weighting is often used which decreases the importance of the feature.

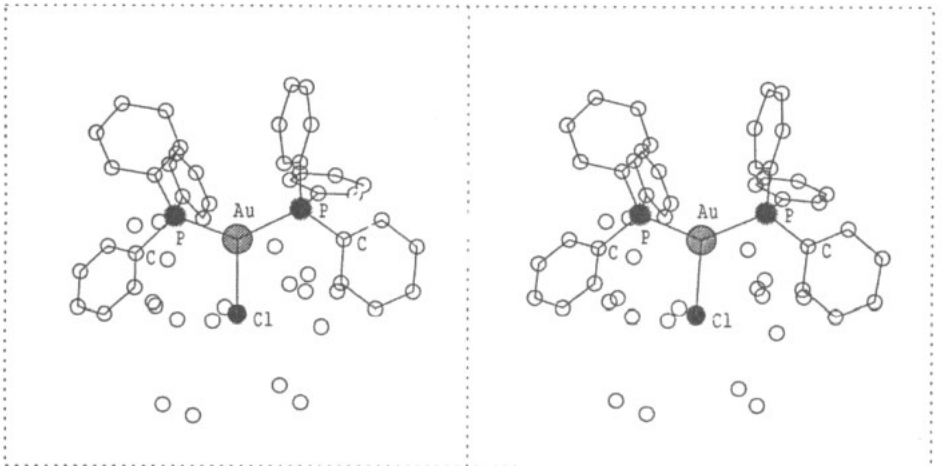

Figure 7. Stereoscopic direct view of the environment of the Au atom in $Au(PPh_3)_2Cl$ up to 6.0 Å, the molecular unit is evidenced by the chemical bonds reported as solid lines.

3.4. $Au(PPh_3)_2Cl$

The second compound that we are going to present is fairly similar to the previous one, being a molecular solid with single units composed of Au, Cl and PPh_3 elements. The crystal structure of $Au(PPh_3)_2Cl$ has been studied both for unsolvated crystals [25], at 295 K, and for benzene solvated specimens [26], both with the $P\bar{1}$ space group. There are two molecules in each unit cell. The molecular geometrical parameters are only slightly different between the two crystalline structures. A stereoscopic view of the environment of the Au atom up to 6.0 Å is shown in figure 7. Intermolecular contacts, as seen from the Au atom, are relatively long distance. The major structural difference with respect to $Au(PPh_3)Cl$ is the presence of two PPh_3 ligands instead of one, and what is even more important for the EXAFS analysis, the absence of any collinearity between the ligand positions. Another significant difference is in the Au–Cl distance that is about 2.53 Å, which is about 0.2 Å longer than in $Au(PPh_3)Cl$, while the distances of the two covalent bonds Au–P are again about 2.23 Å. These Au–ligand distances are very close to those we have resolved in $Au_{55}(PPh_3)_{12}Cl_6$ [13].

A fit of the $k\chi(k)$ signal of the 80 K spectrum has been performed according to the previously described criteria and the results are presented in figure 8. In this case account has been taken of the presence of the $[2p_{3/2}4f]$ excitation channels, that, if neglected, would have produced results similar to those shown in figure 4. A complete summary of the double-electron background shapes in all of these compounds will be reported in section 4.

In figure 8 the first signal from the top, that dominates the spectrum, accounts for the two Au–P bonds. The second weaker Au–Cl signal presents a different phase with respect to the previous compound due to the slightly longer distance. For this reason the envelope of the experimental $k\chi(k)$ is characterized by a typical shape with a very small maximum at 5.5 $Å^{-1}$. This makes the signal extremely sensitive to the actual distribution in ligand distances. The third signal from the top accounts for the Au–C contributions; because of the presence of six phenyl rings, there are six second-neighbour C atoms, split into two shells due to the phenyl ring positions. The C signal in this compound is accordingly found to be more important than in the previous one. The agreement between total calculated signal and

experimental data is again very good, showing a residual dominated by the experimental noise.

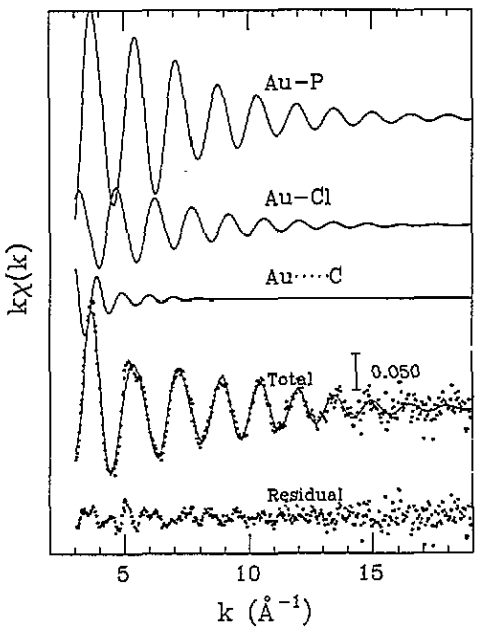

Figure 8. Best fit of the Au L_3 edge spectrum of $Au(PPh_3)_2Cl$ at 80 K. Each two-body contribution is reported as indicated by the labels. The comparison between total experiment and model signals is excellent, and the residual substantially contains experimental noise only.

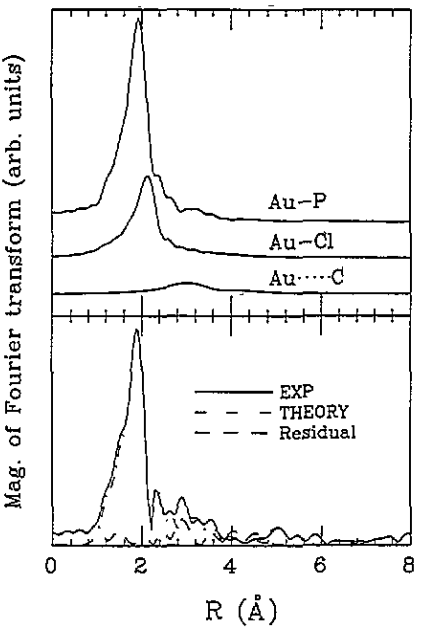

Figure 9. Magnitude of the Fourier transform of the signals reported in figure 8. Compare the absence of a well defined high-frequency MS contribution like the one visible in figure 6 around 4 Å.

The magnitude of the Fourier transform of the various contributions as well as of the total and residual signals is shown in figure 9. A main feature, to be stressed here, is the absence of a high-frequency peak associated with MS contributions of the type visible in figure 6. In this compound an almost complete agreement with experimental data is obtained without accounting for MS effects, because of the absence of linear P–Au–Cl units. The values of the refined structural parameters are reported in table 2 and compared with the crystallographic values. In addition to the L_3 data the analysis has been performed also on the L_2 edge spectrum (80 K) for comparison. The results at the two edges are perfectly compatible although in this case they differ slightly from the crystallographic ones. It should be noted, however, that the comparison is performed at different temperatures and bond length adjustments of a few hundredths of an Ångström are possible between 80 K and 300 K.

We have been investigating the sensitivity of the EXAFS signal to determine independently the composition of the first-shell environment. A fit leaving the coordination numbers to float found 2.08 P atoms and 1.36 Cl atoms. The former value indicates a very strong sensitivity to the actual majority set of neighbours; the relatively larger Cl coordination number reflects the large correlation between this parameter and σ^2, in fact the Au–Cl σ^2 was found to increase in the latter fit. Obviously if fractional coordination

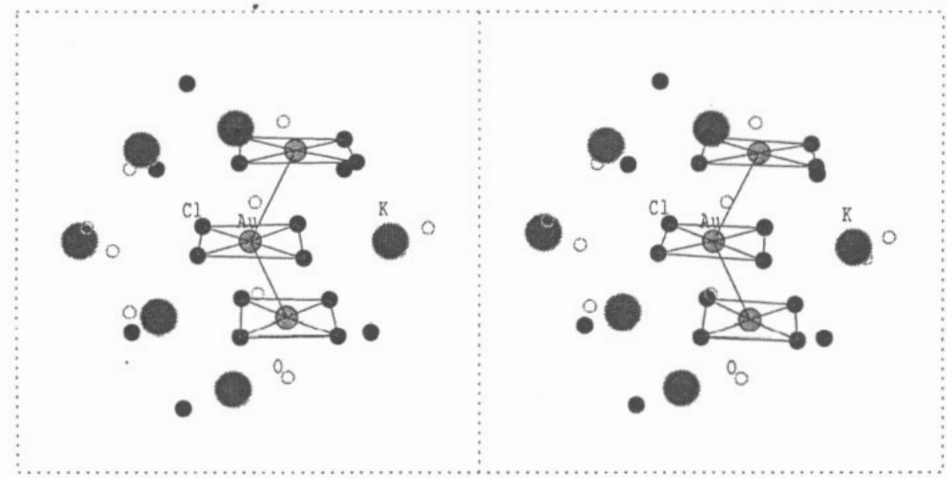

Figure 10. Stereoscopic direct view of the environment of the Au atom in $KAuCl_4 \cdot 2H_2O$ up to 6.0 Å; the molecular $(AuCl_4)^-$ unit is evidenced by the chemical bonds reported as solid lines.

Table 2. Structural parameters for the $Au(PPh_3)_2Cl$ molecule derived in the present EXAFS analysis and comparison with crystallographic results.

Configuration	Parameter	(units)	Crystal structure	L_3 80 K	L_2 80 K
Au–P	R	(Å)	2.331	2.315(10)	2.31(2)
	σ^2	(10^{-4} Å^2)		20(10)	<40
Au–Cl	R	(Å)	2.500	2.528(10)	2.53(5)
	σ^2	(10^{-4} Å^2)		30(20)	<150
Au–C	R	(Å)	3.39	3.5(1)	3.6(2)
	σ^2	(10^{-4} Å^2)		300(100)	

numbers are not allowed EXAFS is perfectly able, in this case, to tell the exact composition of the ligand shell.

A second feature that has been investigated is the topology of the minima under exchange of the atomic species. Provided that three atoms are clearly needed to explain the envelope of the experimental signal, then because of the similarity of the atomic numbers between P and Cl, there are six possible different arrangements of the atoms. These are, for the short and long distance respectively, 2P+Cl (the correct combination), 2P+P, 2Cl+P, PCl+Cl, PCl+P and finally 2Cl+Cl. All of these six combinations have a comparable minimum in the residual, although the lowest residual is given by the correct combination. If nothing is known about the compounds the differences between the minima would be too small to establish the actual composition. However, other chemical insight is helpful. Firstly, the 2:1 ratio of phosphorus to chlorine can be established by standard chemical analysis techniques. Secondly, the range of Au–P covalent bond distances is narrow, especially for compounds of Au^I [38], and they can just fit in the short neighbour shell; thus three of the above possibilities are really ruled out by distance constraints. In general it is found that the distances and σ^2 adjust themselves to unreasonable values if an erroneous composition is chosen. This feature can again be used to select the most reasonable composition in an unknown case. Similar problems in the EXAFS refinement of compounds having short and

long Au–Cl bonds have been discussed elsewhere [15].

3.5. $KAuCl_4 \cdot 2H_2O$

The third compound studied was the hydrated gold chloride salt $KAuCl_4 \cdot 2H_2O$. The $(AuCl_4)^-$ units have a characteristic planar square configuration with the Au in the middle. This compound is quite interesting due to the extreme gold oxidation state that is reached (Au^{III}) and in fact the near-edge structure develops a very sharp white line (figure 1), that is rather unusual for Au L edge spectra.

The crystal structure of $KAuCl_4 \cdot 2H_2O$ [27] follows the *Pbcn* space group with eight equivalent $(AuCl_4)^-$ units in the unit cell. A stereoscopic view of the environment of the Au atom up to 6.0 Å is shown in figure 10. The most interesting characteristic of this compound in the context of the structural configurations relevant to the EXAFS analysis is the presence of the rather regular square planar $(AuCl_4)^-$ unit. The average Au–Cl distance is around 2.29 Å. Such a planar square configuration is known to be subject to large MS effects corresponding to the two diagonal Cl–Au–Cl configurations, and to a lesser extent also to the four distinct orthogonal Cl–Au–Cl triangles. More distant atoms, not directly bonded with the central Au, are two Cl at 3.42 Å, two Au at 3.99 Å and two other Cl at 4.43 Å. The first K atom is not found until 4.48 Å. All these components have been calculated and included in the final fit of the 80 K L_3 data, that is presented in figure 11. The intensities of the various signals indicate that the spectrum is dominated by the low-frequency single-scattering contributions of the four Cl atoms, but in the high-frequency region an MS component becomes visible and actually dominates over the single-scattering ones. The frequency content of each contribution and that of the total model and experimental signals are visualized in figure 12. The overall quality of the fit is again excellent, indicating that by taking proper account of the MS effects it is possible to extend the upper distance limit of the data analysis far beyond the first-shell distance. The inclusion of the Cl–Au–Cl in the fit provides a significative reduction of the residual value.

Table 3. Structural parameters for the $KAuCl_4 \cdot 2H_2O$ hydrated salt at 80 K derived in the present analysis and comparison with crystallographic results.

Configuration	Crystal R (Å)	EXAFS R (Å)	σ^2 (10^{-4} Å^2)
Au–Cl	2.284 2.291	2.286(4)	17(4)
Au–Cl	3.419	3.39(4)	100(50)
Au–Au	3.990	4.0(2)	>50
Au–Cl	4.426	4.5(2)	>20
Au–K	4.488	4.48(4)	<90
	θ (deg)	θ (deg)	σ_θ^2 (deg^2)
Cl–Au–Cl	180	180(f)	<140

This compound and a set of aqueous chloride solutions at different concentrations and pH values was the subject of a recent paper focused on the geochemical aspects relevant to hydrothermal ore transport and deposition of Au [28]. The reported spectrum of $KAuCl_4 \cdot 2H_2O$ is quite similar to ours, and the Fourier transform presents the long-distance peak at about 4 Å. This peak is visible also in acid gold chloride solutions, and was assigned to a long Au–Cl contribution. In the present investigation we have demonstrated

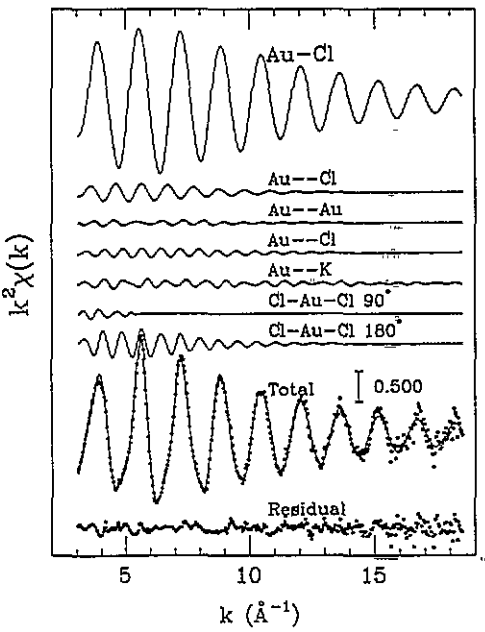

Figure 11. Best fit of the Au L_3 edge $k^2\chi(k)$ spectrum of $KAuCl_4{\cdot}2H_2O$ at 80 K. The spectrum is dominated by the Au–Cl single-scattering signal, but also a strong MS signal due to the Cl–Au–Cl collinear configurations in the $(AuCl_4)^-$ unit is observed. The comparison between total experiment and model signals is excellent, and the residual contains substantially experimental noise only.

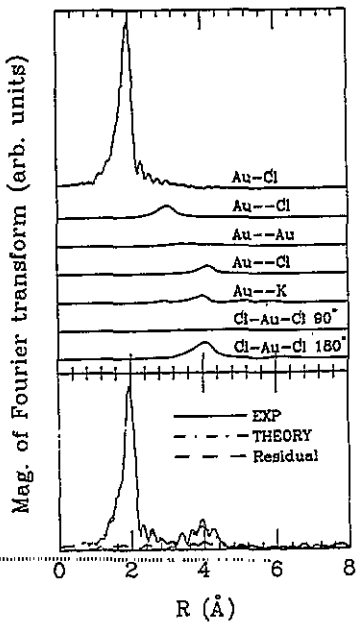

Figure 12. Magnitude of the Fourier transform of the signals reported in figure 11. The presence of a well defined high-frequency MS signal from collinear Cl–Au–Cl configurations, that is the main contribution in the peak around 4 Å, is evident.

that this assignment is erroneous. By far the major component of the peak is actually due to the Cl–Au–Cl three-body MS contribution. This example shows again the importance of accounting for MS effects in EXAFS data analysis. The presence of the 4 Å peak is actually a signature for the presence of a rigid $(AuCl_4)^-$ unit, and the fact that it is visible in acid aqueous solutions indicates the nature of the majority ionic species and actually supports the conclusions drawn in [28].

The final refined parameters from the EXAFS analysis are compared with crystallographic values in table 3. It should be first pointed out that in this case due to the strength and extension in k space of the Au–Cl first-neighbour signal it is possible to derive the Au–Cl parameters with extremely high accuracy. The correlated error in the bond length is only 0.004 Å, and the refined value is in spectacular agreement with diffraction results. The structural disorder of the two slightly inequivalent distances is negligible with respect to the thermal disorder, so that EXAFS finds a single Gaussian peak. The average EXAFS distance is only 0.0015 Å from the average diffraction distance, providing strong evidence that the theory is not affected by systematic errors. Also a very precise determination of the Au–Cl mean square vibrational amplitude could be performed. The value reported in table 3 coincides with the zero-point vibration limit of an Au–Cl bond vibrating with an effective Einstein frequency of about 350 cm^{-1}, the accepted vibrational frequency for this unit [38]. This again demonstrates the reliability of the theoretical standards. We successfully refined

the parameters for the two Cl atoms at 3.4 Å from the Au. However, the errors in the bond lengths of the other pair contributions are rather large as expected due to the weakness of their signals; in practice these atoms cannot be located accurately by EXAFS. The MS signal that dominates the 4 Å peak in the FT is essential to establish (from EXAFS data) the existence of the precise Cl–Au–Cl alignment with minor thermal vibrations inducing a bond angle mean square vibrational amplitude no greater than 140°[2].

4. Double-electron excitation evidence

In this section we summarize the experimental evidence for multi-electron excitation background effects obtained in the present investigation. The experimental background that was revealed in $Au(PPh_3)Cl$ after suppression of the structural signal has been shown in figure 4. Similar spectra have been obtained, independently of the temperature, for the other compounds and edges investigated. A comprehensive picture of the background anomalies discovered for these Au compounds is reported in figure 13. The spectra reproduce the residual absorption coefficient $\Delta\alpha$, in excess with respect to the structural signal and the smooth polynomial spline, multiplied by k as a function of the energy above the L_3 inflection point. The comparison between the various curves, related to different compounds and different L edges, indicates that there are several common features occurring at precise energies. First of all, all of the L_3 and L_2 spectra show at ΔE=110±5 eV the slope change associated with the simultaneous excitation of a 2p and a 4f electron, that leaves the core in a [2p4f] double-hole configuration. This energy, indicated with a vertical dashed line in figure 13, is found to be in very close agreement with theoretical estimates based on ΔSCF calculations [20]. The only reported L_1 spectrum presents around this energy a broad maximum. While the reported shape is certainly the one mostly affected by noise, we point out that it shows a resemblance with the one measured for the L_1 edge of Hg vapours [20].

Another feature with unknown origin seems to occur systematically around 180 eV; it is indicated with a vertical dotted line in figure 13. The energy is close to the sum of the two additional excitation energies for 5p and 4f electrons and for this reason could be due to a triple-electron excitation. The additional energy is also close to the binding energy of a 2p electron in Cl, therefore another process that should be possibly considered is the simultaneous excitation of two core electrons in the two bonded atoms.

The multielectron excitation background presents remarkable differences in intensity and shapes among the various compounds, in particular all of the features appear strongly enhanced and sharpened in the $KAuCl_4{\cdot}2H_2O$ case, reflecting the sharpening of any near-edge feature. This is in line with the rather general observation that the higher the oxidation state the stronger the cross-sections of double-electron processes. The slope discontinuity at the [2p4f] threshold is in $KAuCl_4{\cdot}2H_2O$ about five times larger than in $Au(PPh_3)Cl$, at the same time the 180 eV feature is strong (although the curves are k weighted) and at least another clear step is evident around $\Delta E = 60 \pm 5$ eV (arrow in figure 13). The energy coincides with the additional energy required to excite the $5p_{3/2}$ electron, another smaller feature around 80 eV could be similarly associated with the further excitation of a $5p_{1/2}$ electron. There are no clear indications of equivalent features in the other compounds suggesting that these particular channels are strongly enhanced in Au^{III} compounds.

It is clear that all these results have a considerable applicative potential in improving the structural EXAFS data analysis at the Au L edges. The following conclusions can be outlined.

(a) It is only by accounting for the double-electron excitation background that fitted

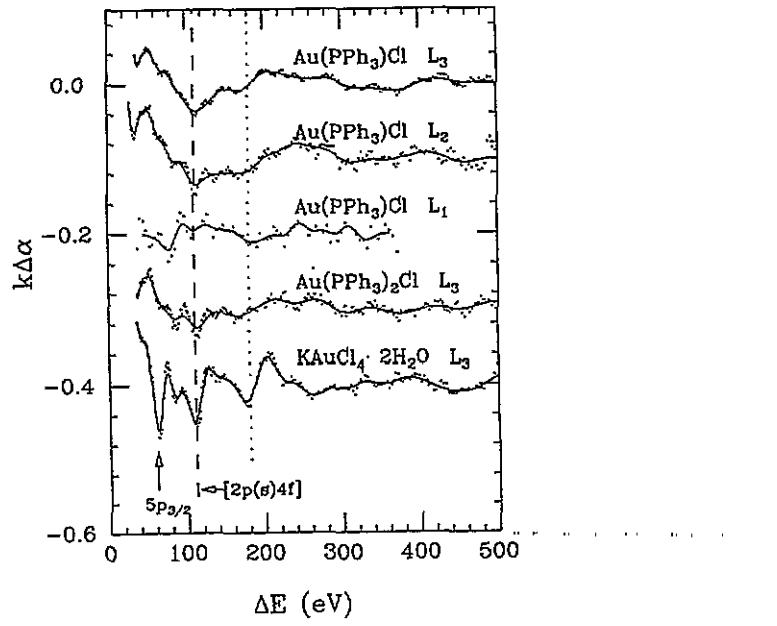

Figure 13. Background anomalies $k\,\Delta\alpha$, not explained by the structural signal, as a function of the energy above the L edge ΔE, for the various compounds investigated. The similarities between the $k\,\Delta\alpha$ signals are evident, and the presence of a cusp around $\Delta E = 110$ eV associated with the [2p4f] double-electron excitation threshold is undoubtedly confirmed.

residuals affected only by experimental noise can be obtained, and unphysical peaks in the Fourier transform removed.

(b) Failure to account for the background features may result in an erroneous determination of the structural parameters expecially in cases with weak and correlated structural signal.

(c) Empirical background models are suitable to describe the double-electron channel discontinuity; however, any theoretical insight in position, intensity and shape of their cross-section is extremely welcome.

5. Conclusions

In the present paper we have addressed the problem of assessing the validity of our advanced EXAFS data analysis at the Au L edges based on the comparison between crystallographic data and EXAFS refinements for three model compounds.

Several conclusions can be drawn.

(1) The importance of accounting for the correct background model including double-electron excitation effects has been clearly shown.

(2) We have demonstrated that it is possible to perform a reliable analysis at all the Au L edges based on theoretical signals including single- and multiple-scattering effects.

(3) The structural refinements were found to be in excellent agreement with crystallographic results. The EXAFS signal was found to be sensitive to the position of P and Cl ligands, and it was found to be possible to detect the Au–P and Au–Cl bond distances to better than 0.01 Å. The EXAFS signal was sensitive to the existence of linear geometries which maximize the intensity of multiple-scattering effects.

(4) It has been shown that with this analysis based on theoretical standards it is possible to determine the absolute mean square vibrational amplitudes of Au–P and Au–Cl bonds, with an overall error only limited by the experimental noise. These σ^2 values are exactly consistent with estimates based on the known vibrational frequencies.

The method of analysis reported in the present paper will be useful for all future applications of EXAFS spectroscopy at the Au L edges. This can be relevant to several scientific contexts such as medical and geochemical fields, as well as structural analysis of coordination and cluster compounds of gold.

Acknowledgments

The research has been partly supported by EC Science Plan contract No SC1*-CT92-0788 (AF) and the Royal Society (REB). We thank the SERC staff for operating the storage ring. We wish to acknowledge the use the use of the SERC's Chemical Database Service (CSSR) at Daresbury. Thanks are due to N V Russell (Chemical Laboratory, University of Kent at Canterbury) for helping us in the data collection.

References

[1] Greenwood N N and Earnshaw A 1984 *The Chemistry of the Elements* (Oxford: Pergamon) ch 28
[2] Puddephatt R J 1978 *The Chemistry of Gold* (Amsterdam: Elsevier)
[3] Mazid M A, Razi M T, Sadler P J, Greaves G N and Gurman S J 1980 *J. Chem. Soc. Chem. Commun.* 1261
Frank C Shaw III, Schaeffer N A, Elder R C, Eidsness M K, Trooster J M and Calis G H M 1984 *J. Am. Chem. Soc.* **106** 3511
Elder R C, Ludwig K, Cooper J N and Eidsness M K 1985 *J. Am. Chem. Soc.* **107** 5024
[4] Hall K P and Mingos D M P 1984 *Prog. Inorg. Chem.* **32** 237
[5] Turkevich J, Stephenson P C and Hillier J 1951 *Discuss. Faraday Soc.* **11** 55
[6] Baschong W, Lucocq J M and Roth J D 1985 *Histochemistry* **83** 409
[7] Schmid G, Pfeil R, Boese R, Bandermann F, Meyer S, Callis G H M and van der Velden J W A 1981 *Chem. Ber.* **114** 3634
[8] Schmid G 1992 *Chem. Rev.* **92** 1709
[9] Thiel R C, Benfield R E, Zanoni R, Smit H H A and Dirken M W 1993 *Struct. Bonding* **81** 1
[10] Fairbanks M C, Benfield R E, Newport R J and Schmid G 1990 *Solid State Commun.* **73** 431
[11] Marcus M A, Andrews M P, Zegenhagen J, Bommannavar A S and Montano P 1990 *Phys. Rev.* B **42** 3312
[12] Cluskey P D, Newport R J, Benfield R E, Gurman S J and Schmid G 1992 *Chemical Processes in Inorganic Materials: Metal and Semiconductor Clusters and Colloids (Proc. Mater. Res. Soc. 272)* ed P D Persans, J S Bradley, R R Chianelli and G Schmid (Pittsburgh, PA: Materials Research Society) p 289
[13] Cluskey P D, Newport R J, Benfield R E, Gurman S J and Schmid G 1993 Z. *Phys.* D **26** S8
[14] Sinfelt J H and Meitzner G D 1993 *Acc. Chem. Res.* **26** 1
[15] Elder R C and Watkins J W II 1986 *Inorg. Chem.* **25** 223
[16] Schaphorst S J, Kodre A F, Ruscheinski J, Crasemann B, T. Åberg, Tulkki J, Chen M H, Azuma Y and Brown G S 1993 *Phys. Rev.* A **47** 1953
[17] D'Angelo P, Di Cicco A, Filipponi A and Pavel N V 1993 *Phys. Rev.* A **47** 2055
[18] Burattini E, D'Angelo P, Di Cicco A, Filipponi A and Pavel N V 1993 *J. Phys. Chem.* **97** 5486
[19] Filipponi A, Tyson T A, Hodgson K O and Mobilio S 1993 *Phys. Rev.* A **48** 1328
[20] Filipponi A, Ottaviano L and Tyson T A 1993 *Phys. Rev.* A **48** 2098
[21] Di Cicco A and Filipponi A 1994 *Phys. Rev.* B **49** 12564
[22] Li G, Bridges F and Brown G S 1992 *Phys. Rev. Lett.* **68** 1609
[23] Watkins J W II, Elder R C, Greene B and Darnall D W 1987 *Inorg. Chem.* **26** 1147
[24] Baenziger N C, Bennett W E and Soboroff D M 1976 *Acta Crystalllogr.* B **32** 962
[25] Bowmaker G A, Dyason J C, Healy P C, Engelhardt L M, Pakawatchai C and White A H 1987 *J. Chem. Soc. Dalton Trans.* 1089
[26] Baenziger N C, Dittemore K M and Doyle J R 1974 *Inorg. Chem.* **13** 805
[27] Theobald F and Omrani H, 1980 *Acta Crystallogr.* B **36** 2932

[28] Farges F, Sharps J A and Brown G E Jr. 1993 *Geochim. Cosmochim. Acta* **57** 1243
[29] Kowala C and Swan J M 1966 *Aust. J. Chem.* **19** 547 .
[30] Filipponi A, Di Cicco A, Tyson T A and Natoli C R 1991 *Solid State Commun.* **78** 265
[31] Filipponi A, Di Cicco A and Natoli C R 1994 *Phys. Rev.* B submitted
[32] Filipponi A 1991 *J. Phys.: Condens. Matter* **3** 6489
[33] Benfatto M, Natoli C R, Bianconi A, Garcia J, Marcelli A, Fanfoni M and Davoli I 1986 *Phys. Rev.* B **34** 5774
[34] Tyson T A, Hodgson K O, Natoli C R and Benfatto M 1992 *Phys. Rev.* B **46** 5997
[35] Cyvin S J 1968 *'Molecular Vibrations and Mean Square Amplitudes'* (Oslo: Elsevier)
[36] Messiah A 1954 *Quantum Mechanics* vol I (New York: Wiley) p 448
[37] Stern E A 1993 *Phys. Rev.* B **48** 9825
[38] Puddephatt R J 1978 *'The Chemistry of Gold'* (Amsterdam: Elsevier) p 261